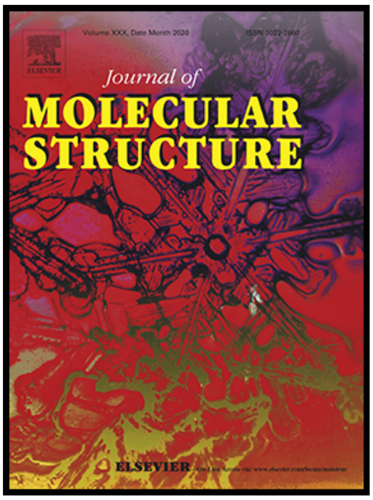

Experimental and Theoretical (DFT) investigation of Crystallographic, Spectroscopic and Hirshfeld surface analysis of anilinium arsenate

N. Kanagathara , F. MaryAnjalin , V. Ragavendran ,
D. Dhanasekaran , R. Usha , R. Gowri Shankar Rao ,
M.K. Marchewka

PII: S0022-2860(20)31289-8
DOI: https://doi.org/10.1016/j.molstruc.2020.128965
Reference: MOLSTR 128965

To appear in: *Journal of Molecular Structure*

Received date: 16 April 2020
Revised date: 23 July 2020
Accepted date: 23 July 2020

Please cite this article as: N. Kanagathara , F. MaryAnjalin , V. Ragavendran , D. Dhanasekaran , R. Usha , R. Gowri Shankar Rao , M.K. Marchewka , Experimental and Theoretical (DFT) investigation of Crystallographic, Spectroscopic and Hirshfeld surface analysis of anilinium arsenate, *Journal of Molecular Structure* (2020), doi: https://doi.org/10.1016/j.molstruc.2020.128965

Highlights

- Synthesis of new anilinium arsenate – new crystalline product
- Single crystal X-ray structure determination and optimization of the grown crystal.
- Theoretical and Experimental Vibrational spectroscopic studies has been carried out
- NBO, HOMO-LUMO, MEP and Hirshfeld surface analysis has been done to understand intermolecular interactions and charge transfer within the molecule.

Experimental and Theoretical (DFT) investigation of Crystallographic, Spectroscopic and Hirshfeld surface analysis of anilinium arsenate

N.Kanagathara[a*], F.MaryAnjalin[a], V.Ragavendran[b], D.Dhanasekaran[c], R.Usha[a],

R.Gowri Shankar Rao[d], M.K.Marchewka[e]

[a] Department of Physics, Saveetha School of Engineering, Saveetha Institute of Medical and Technical Sciences, Thandalam, Chennai 602 105, India.

[b] Department of Physics, Sri Chandrasekharendra Saraswathi Viswa Mahavidyalaya, Enathur, Kanchipuram-631561.

[c] Department of Electronics and Communication Engineering, Saveetha School of Engineering, Saveetha Institute of Medical and Technical Sciences, Thandalam, Chennai 602 105, India.

[d] Department of Physics, Vel Tech Rangarajan Dr.Sagunthala R&D Institute of Science and Technology, Chennai -62.

[e] Institute of Low Temperature and Structure Research, Polish Academy of Sciences, 50-950 Wrocław, 2, P.O. Box 937, Poland.

Corresponding author: kanagathara23275@gmail.com

Cell no: +91 8056107511

ABSTRACT

In the present communication, aniline with arsenic acid molecular complex has been taken as the subject for experimental and theoretical investigation. The anilinium arsenate (ANILAS) – a new crystalline product is grown by slow evaporation technique at room temperature. Density functional theoretical calculations have been computed with Gaussian 09 program. The structure is optimized with DFT/B3LYP-6-311G(d,p) basis set. The vibrational frequencies and electronic properties have been done with the help of Density Functional Theory (DFT) computations. The charge transfer, as well as occurrence of strong inter and intra molecular interactions were confirmed by frontier molecular orbital analysis, natural bonding orbital analysis (NBO) and molecular electrostatic potential. ^{1}H and ^{13}C NMR chemical shift of the studied compound has also been calculated using Gauge Independent Atomic Orbital (GIAO) method. Further, "the 3D Hirshfeld surface analysis and 2D fingerprint maps gives deep insight into the intermolecular interactions between the compound".

Keywords: XRD; FT-IR; FT-Raman; HOMO-LUMO; NBO; Hirshfeld.

1. Introduction

The knowledge of non-covalent interactions in particular hydrogen bonding between the molecules are helpful for the design of new crystalline materials with desired physical, chemical and biological properties which lead to the development of many pharmaceutical products. Since the hydrogen bonding provide an additional stabilizing effect and shape for the crystal lattice, there are many vibrational studies have been reported for hydrogen bonded systems [1-4]. Hydrogen bonded system play a vital role in the structure determination. Aniline and its derivatives are widely used in various industrial and commercial purposes like dyestuff, pesticide and pharmaceuticals. Aniline and its derivatives have been widely used as starting materials for many chemicals, pharmaceuticals, dyes, electro-optical, biological, materials science and many other industrial processes [4-6]. The hydrogen bonding of 23 aniline's derivatives in various solvents and in solid states are studied by many researchers [4-9]. The vibrational spectra of aniline and its derivatives were reported earlier [10-14]. DFT studies on structural and electronic properties of various aniline compounds have been investigated by many researchers [15-19]. Similarly, "there are many reports available for the structural, vibrational and other investigation on arsenic acid with various organic materials" [20-21]. We are reporting the structural and vibrational spectra of aniline with arsenic acid complex for the first time. In the present paper, we have grown a crystal ANILAS (Anilinium Arsenate) by slow evaporation technique and evaluated the role of hydrogen bonding interactions based on structural parameters. Also, “DFT calculations were carried out to predict the results for molecular geometry as well as vibrational frequencies”. Optical and electronic properties have been predicted theoretically. The Natural Bond Orbitals (NBO), frontier molecular orbital analysis and NMR studies were carried out for this title compound. In addition to that we have carried out the vibrational as well as Hirshfeld surface analysis of our synthesized material and their results are discussed in detail.

2. Experimental procedure

The starting compounds, aniline (Aldrich, 99%) and As_2O_5 (Aldrich, 94%) were used as supplied and prepared in the ratio of 1:1. To get arsenic acid (H_3AsO_4), first As_2O_5 was dissolved in water then the dissolved As_2O_5 solution was added drop wise to the solution of aniline and stirred well for about seven hours. After the solution was cooled to room temperature, it remained clear, without any precipitants. Then, the solution was purified with the aid of active charcoal. Active charcoal is a carbon filter commonly used for water purification which boasts a large surface area to capture and store impurities. The solution was slowly evaporated during a few days till the crystals appeared. The photograph as well as reaction scheme of as-grown single crystal of ANILAS is shown in Fig. 1a and 1b respectively.

3. Characterization techniques

3.1 X-ray data collection

A colourless single crystal of the title compound having the edges of 0.21×0.13×0.12 mm^3 was used for data collection on a four circle KUMA KM-4 diffractometer equipped with a two-dimensional area CCD detector. The graphite monochromatized MoKα (λ = 0.71073 Å) and ω-scan technique with $\Delta\omega = 0.75^o$ for one image were used for data collection. Integration of the intensities, correction for Lorenz and polarization effects was performed using KUMA KM-4 CCD software [22]. The face-indexed analytical absorption was calculated using the SHELXTL program [23], the maximum and minimum transmission factors being 0.4973 and 0.6540. A total of 7443 reflections were integrated (2289 independent reflections, R_{int}=0.0230) were used for structure solution and refinement. The structure was solved by direct methods by use of *SHELXL-97* program [24]. Initially, "the structure was refined with isotropic thermal parameters. In final refinement all non-hydrogen atoms were refined with anisotropic thermal parameters by full-matrix least-squares methods by means of SHELXL97 program". Scattering factors for neutral atoms and calculations for anomalous dispersion were as in SHELXL97 program [24]. Fig.2 depicts the ORTEP plot of anilinium arsenate with the atom numbering scheme. Displacement ellipsoids are drawn at 30% probability level. Fig.3 shows the molecular packing of anilinium arsenate forming two dimensional networks viewed along c axis.

3.2 Quantum chemical calculations

Quantum chemical calculations were accomplished using Gaussian 09 program with B3LYP/6-311G(d,p) basis set to anticipate the structure and vibrational wavenumbers of the grown crystal [25]. Single crystal X-ray diffraction data is used as input to perfrom the calculations. Fig.4 depicts the optimized structure of ANILAS. In DFT computations on vibrational spectra, generally scaling procedures are used to improve the wavenumbers. To correct the calculated harmonic frequencies, infrared and Raman intensities, all the frequencies were scaled by 0.9665 [25]. The absence of imaginary wavenumbers on the calculated vibrational spectrum confirms the optimized structure with minimum energy. The NBO calculations were performed using NBO 5.1 program as implemented in the Gaussian 09W package to understand the various second order interactions between the filled and vacant orbital of one subsystem to another subsystem [26]. The Time dependent –Density

Functional Theory (TD-DFT) method is employed to obtain the UV-Visible spectrum. In the case of HOMO-LUMO analysis, graphic illustrations of the isosurface with the value equal to 0.001 was used [27]. MERCURY 3.8 [28] software package was used to generate powder X-ray diffraction pattern of the grown crystal by giving crystallographic information file as the input. The simulated powder X-ray diffraction pattern was calculated from the single crystal structural data (cif file) using the CCDC Mercury software.

3.3 Spectroscopic measurements

The vibrational measurements were carried out at room temperature. Infrared spectra were taken with a Bruker IFS-88 spectrometer in the region 4000-80 cm^{-1} while powder Fourier Transform Raman (FT-Raman) spectra were taken with an FRA-106 attachment to the Bruker IFS-88 spectrometer equipped with Ge detector cooled to liquid nitrogen temperature. Resolution was set up to 2 cm^{-1}, signal/noise ratio was established by 32 scans, weak apodisation. Nd^{3+}: YAG air-cooled diode pumped laser of power of 200mW was used as an exciting source. The incident laser excitation is 1064 nm. The scattered light was collected at the angle of 180° in the region 3600-80 cm^{-1}, resolution 2 cm^{-1}, 256 scans. Due to the poor detector response, the Raman counterparts of the infrared bands located above 3200 cm^{-1} are not observed in the spectrum.

3.4 Molecular Hirshfeld surface calculations

Hirshfeld surface analysis is a powerful tool to study the intermolecular interactions of the molecular crystals. The size and shape of Hirshfeld surface provides visualization of intermolecular close contact in molecular crystals [29]. It is used to obtain the 3D Hirshfeld surfaces and 2D finger plots of the title compound by giving cif as the input using Crystal Explorer 3.1 software [30]. Hirshfeld surfaces are constructed based on electron distribution which is calculated as sum of spherical atom electron densities [31]. The normalized contact distance dnorm based on the distance from a point on the surface to the nearest nucleus outside the surface, *d*e is the distance from a point on the surface to the nearest nucleus inside the surface, *d*i enables the identification of the regions of particular importance to the intermolecula rinteractions. The intermolecular contacts in the crystal lattice is provided by the combination of de and di in the form of two-dimensional fingerprint plot [32]. It helps to generate Hirshfeld surfaces that mapped with dnorm, shape index, curvedness and 2D fingerprints. The normalized contact distance dnorm = d_i - r_i^{vdw} / r_i^{vdw} + d_e - r_e^{vdw} / r_e^{vdw} where r_i^{vdw} and r_e^{vdw} are the van der Waals radii of the atoms.The intermolecular contact is shorter than r^{vdw} if dnorm is negative and longer if dnorm is positive. The red-white-blue colour in Hirshfeld surface map represents the shortest intermolecular contact, contact around r^{vdw} separation and longer intermolecular contact distance respectively. The 2D fingerplot is a combination of d_e and d_i provides the summary of intermolecular contacts in the crystal and are in complement to the Hirshfeld surfaces [33]. The shape index and curvedness are the two coloured properties can also be specified based on the local curvature of the surface.

4. Results and Discussion

4.1 Optimized geometry description

Single crystal X-ray diffraction analysis reveals that the grown crystal crystallizes in monoclinic system with centro symmetric space group P 21/c with primitives a= 9.872(2)Å, b= 10.769(2)Å, c = 8.223(2) Å and interfacial angles α=γ=90° and β=92.23(3)°. Details of the data collection parameters, crystallographic data and final agreement factors are collected in the Table 1. Selected bond distances and angles along with DFT/6-311G(d,p) results are listed in Table 2.The asymmetric unit of anilinium arsenate is formed by the one protonated anilinium cation and one deprotonated arsenate anion. The primitive cell consists of 4 molecules. The phenyl ring is nearly planar and the nitrogen atoms of the $–NH_3$ ammonium group lies on the ring mean plane. The nitrogen atom N1 deviates by 0.011(2) Å from the mean plane of the ring (C1─C6). The phenyl ring (C1─C6) adopts a usual planar conformation with C3 atom having a deviation of 0.004(1)Å. All C-N bond angles are in the range 119-120^{o}. Whereas the Carbon atom C1attached to the nitrogen atom N1 describes an angle 121.60^{0} with C2 and C6 atom [34]. The crystal structure is stabilized by intra and intermolecular N─H···O and O─H···O hydrogen bonds which generate a two dimensional network. A related structure of melaminium arsenate was reported by Anbalagan et al [20]. There is a significant increase in the N1-H13 bond length (0.924 Å) of ammonia group attached to the aniline ring. The arsenic atom (As1) bonded to four oxygen atoms with significant variation in the bond length [As1-O1=1.724 Å; As1-O2=1.658 Å; As1-O3=1.713 Å; As1-O4=1.655 Å]. The As1-O1 bond which is engaged in strong hydrogen bond [H11···O1 = 0.85(3) Å] is elongated due to protonation. Hydrogen bonding parameters are listed in Table 3. Significant variation in the bond angles of Arsenic atom attached to the two carbon atoms i.e O2-As1-O2 = 110.73; O1-As1-O3=96.58; O3-As1-O4=111.38 whereas O4-As1-O2=115.86. The oxygen atoms O1 and O3 attached to Hydrogen atoms H111 and H311 bond angle is shortened whereas other bond angles are increased. This variation confirms the transfer of hydrogen from arsenic to aniline molecule i.e deprotonation. All the bond angles and bond distances are within the expected range [35-38]. The obtained parameters are well in agreement with theoretical values. Atomic displacement parameters tabulated in Table 4. Fractional atomic coordinates and isotropic or equivalent isotropic displacement parameters are tabulated in Table 5.

4.2 Powder X-ray diffraction analysis

Powder X-ray diffraction (XRD) analysis was performed theoretically to identify the crystalline nature of the grown crystal. The results of XRD are calculated with the help of Mercury 3.8 software [28]. Fig.5 depicts the calculated XRD pattern of the grown crystal. The crystallite size (D) of ANILAS was determined by Debye-Scherrer's formula using equation

$$D= K\lambda/(\beta_{1/2}\cos\theta) \qquad \_\_\_\_\_\_\_\_\_\_\_\_\_\_ \qquad (1)$$

where $K=0.89$; $\lambda=1.5405$ Å and $\beta_{1/2}$ is the peak width of the reflection at half intensity. The maximum intensity peak occurs at $2\theta=21.54^{o}$. As the powder sample was used for XRD, the effect of the strain, instruments and other unknown factor causing the broadening of the peak were ignored. The average value of the crystallite size of ANILAS is found to be 14.089 μm.

4.3 Vibrational spectroscopic analysis

The study of vibrational spectroscopic analysis of organic compounds is considered as one of the most significant task in the field of organic chemistry. Probable assignments to the observed bands have been made with the help of magnitude and intensities of the recorded spectra. Room temperature powder infrared and Raman measurements for the aniline arsenic acid molecular complex (1:1) has been recorded and discussed in detail. The assignments made in the present study are in good agreement with the earlier assignments as well as theoretical results proposed by several investigators on some similar type of molecules. The observed frequencies of anilinium arsenate along with their relative intensities and probable assignments are presented in Table 6. The characteristic overtones are seen from about 2300-1900 cm^{-1}. The interpretation of the both IR and Raman spectra of ANILAS is presented and discussed in detail in this communication. Figure 6 and 7 gives the experimental and theoretical FT-IR and FT Raman spectrum of ANILAS.

4.3.1 N-H vibrations

The vibrations of hydrogen manifest themselves as NH_3^+ group vibrations of anilinium cation with weak interactions. According to crystallographic data there are three N-H···O type of hydrogen bonds with an average length of 2.750 Å. Infrared spectrum of N-H stretching frequencies in the region 3100-2800 cm^{-1} and multiple combination bands in the 2900 - 2000 cm^{-1} which are the prominent IR bands of protonated amine salts of aniline derivatives [39]. The strong infrared peaks at 2854, 2773 and 2625 cm^{-1} are assigned to N-H···O stretching. The Raman absorption at 3390 cm^{-1} with medium intensity is assigned to NH_3^+ asymmetric stretching of anilinium cation. Theoretically, "this peak is observed at 3402 cm^{-1}". The infrared peaks at 1795 and 1742 cm^{-1} are assigned to N-H_3 asymmetric bending plane of vibration whereas the infrared peaks at 1702 and 1692 cm^{-1} with weak intensity is assigned to N-H_3 in-plane bending vibration". Theoretically, "this peak is observed at 1660 cm^{-1}. The medium infrared peak at 1628 cm^{-1} and broad Raman peak with weak intensity at 1627 cm^{-1} are ascribed to NH_3^+ in-plane bending vibration". The strong infrared peak at 1602 cm^{-1} is attributed to NH_3^+ out-plane bending vibration [26]. Its corresponding Raman counterpart occurs at 1604 cm^{-1}. DFT computes this assignment at 1612 cm^{-1}. The weak peaks at 581, 531 and 532 cm^{-1} in FT-IR and FT Raman are attributed to NH_3 torsional vibration respectively.

4.3.2 C-H vibrations

The prominent bands of aromatic compounds usually occurs at five regions of the infrared spectrum viz. 3100-3000 cm^{-1} (C-H stretching). 2000-1700 cm^{-1} (overtones and combinations), 1650-1430 cm^{-1} (C=C stretching), 1275-1000 cm^{-1} (in-plane C-H deformation) and 900-690 cm^{-1} (out-of-plane C-H deformation) [40]. In general, N-H and C-H vibrations are in the higher frequency region than C-O and C-N vibration. The carbon-hydrogen stretching occurs in the region 3100-3000cm^{-1} and in this region the bands are not affected appreciably by the nature of the substituent [41]. NH and CH stretching frequencies are expected to occur in the higher frequency region [42]. There are multiple weak bands in the region 3100-3000 cm^{-1} due to aromatic C-H stretching vibrations in aromatic compounds [43] and this weak in intensity is due to the decrease of dipole moment caused by the reduction of negative charge on the carbon atoms. This reduction occurs because of the electrons withdrawing on the carbon atoms by the substituent due to the decrease of inductive effect, which in turn is caused by the increased chain length of the substituent [40]. The strong infrared peak at 3056 cm^{-1} and 3064 cm^{-1} in FT Raman spectrum is assigned to C-H asymmetric and symmetric stretching vibration respectively. The strong infrared peaks at 2958 and 2928 cm^{-1} is assigned to C-H symmetric stretching vibration. The peak at 1456 cm^{-1} with strong intensity is assigned to C-H stretching vibration [12]. There are several peaks observed in the region 1377-1328 cm^{-1} and are attributed to C-H in-plane bending vibration and O-H in-plane bending vibration. The weak IR peaks at 1176 and 1132 cm^{-1} with Raman counterpart at 1170 and 1329 cm^{-1} is assigned to C-H in-plane bending.The strong infrared peak at 1210 cm^{-1} is attributed to C-H out plane bending vibration. The corresponding Raman peak is observed at 1211 cm^{-1}. Medium infrared peak at 998 cm^{-1} is assigned to C-H out plane bending vibration. The weak Raman peak at 830 cm^{-1}is assigned to C-H out-plane bending vibration [44]. The very strong IR peak at 771 cm^{-1} is attributed to C-H out plane bending vibration.

4.3.3 C-N vibrations

It is very difficult to assign C-N stretching since mixing of several bands is possible in this region. Silverstein et al [39] assigned the C-N stretching absorption in the region 1382-1266 cm^{-1} for aromatic amines. Upon ionization of aniline, the C-N bond significantly shortens due to an increased conjugation between the planar NH_2 group and the ring. The weak Raman peak at 1249 cm^{-1} and medium IR peaks at 1191 and 1167 cm^{-1} and Raman peak at 1183 cm^{-1} is assigned to C-N stretching. DFT compute this peak at 1171 cm^{-1}. C-N out-of-plane bending is observed at 460 cm^{-1} in Raman spectrum.

4.3.4 C-C vibrations

The C-C stretching occurs at 1592 and 1581 cm^{-1} in IR with strong intensity. The strong infrared peak at 1498 cm^{-1} with its weak Raman counterpart at 1508 cm^{-1} is assigned to C-C stretching of aniline ring. The medium IR peak at 1295 cm^{-1} is due to the ring stretching of anilinium cation, but it generally occur at 1306 cm^{-1}. This position change is due to the self-association of intermolecular interactions. Experimental infrared spectrum shows strong peak at 1032 cm^{-1} which is assigned to C-C-H in-plane bending vibration. Its corresponding Raman peak occurs at 1027 cm^{-1} with very weak intensity. DFT computes this assignment at 1050 cm^{-1}. The very strong IR peak at 1006 cm^{-1} is due to C-C stretching or C-C-C in-plane bending vibration. The strong IR peak occurs at 689 cm^{-1} is due to ring deformation. Theoretically, “this peak is computed at 1017 cm^{-1}”.

4.3.5 As-O/As-OH vibrations

The hydroxyl groups are generally observed around 3500 cm^{-1} and this band is highly intense and broader than free OH vibration because of intermolecular hydrogen bonding. Theoretically, "observed peaks at 3700 and 3698 cm^{-1} is due to O-H asymmetric stretching of arsenate anion". Arsenate ion in solution exhibit tetrahedral symmetry gets distorted due to protonation. As a result, vibrations of arsenate ion occur at lower wavenumbers [20, 45]. The infrared spectra of various organo arsenic compounds were studied by Petitt and Tharun [46]. Vibrational spectra of arsenate anions exhibit As-O and As-OH vibrations. According to Frost et al the calculated infrared peak at 996 cm^{-1} is assigned As-OH in plane bending vibration. For C3v symmetry there are three vibrations expected for As-O stretching in the region 900-700 cm^{-1} [47]. Since the stretching force constant of As-O bond is higher than As-OH bond, the highest frequency is assigned to the symmetrical AsO3, stretching mode and the lower to the As-O(H) stretching. The band at 863 cm^{-1} is assigned to the asymmetrical AsO_3, stretching. The corresponding calculated peak occurs at 856 cm^{-1}. The IR/Raman band observed at 751/754 cm^{-1} is ascribed to As-O stretching vibration. This frequencyiscomputedat734 cm^{-1}.In the region of the O-As-O deformation modes (500-200 cm^{-1}) three bands are expected from C3v symmetry. The IR peaks at 490 and 414 cm^{-1} is attributed to O-As-O deformation modes of vibration. Its corresponding Raman peak is found at 407 and 279 cm^{-1} [47]. Theoretically, "these peaks are observed at 334, 328,283,279, 261,253 and 216 cm^{-1}".

4.4 NBO analysis

NBO analysis is used to study the intra and inter molecular interactions between the molecules [26]. The selected donor-acceptor interactions based on second order perturbation Fock – matrix theory is listed in Table 7. The delocalization of electron from filled Lewis type NBO to non –Lewis type NBO results in hyper conjugation effect.

For each donor (i) and acceptor (j), the stabilization energy E(2)

$$E_2 = \Delta E_{ij} = q_i \frac{F(i,j)2}{Ei-Ej} \qquad \text{------------ (2)}$$

Where q_i is the occupancy of donor orbital, E_i and E_j are energies of donating and accepting orbital's and F(i,j) is the NBO Fock matrix elements [48-49].

In the title compound, it is seen from Fig. 8 that all the carbon atoms in aniline have negative charge except 12C which is attached to the amino group has a positive charge of 0.132e. Similarly, "in arsenate anion, all the oxygen atoms have a negative charge ~ -1.045e". The remaining atoms arsenic (2.332e) and hydrogen atoms (0.487e) carry positive charge. All the carbon atoms of phenyl group have negative charge whereas the carbon atom which is attached to the amino group has positive charge (0.132e). The strongest intra molecular interaction energy is found to be 119.09 KJmol^{-1} which is due to the electrons donated from lone pair of oxygen atoms O5 to O2 to antibonding arsenic atom results in resonance. This shows that electron cloud can accumulate at arsenate anion which is further confirmed by electrostatic potential studies. The next stabilization energy is 175.32 and 122.38 KJmol^{-1} is due to high intramolecular hyper conjugative interaction of π(C12-C3) to π*(C15-C17) and π(C12-C13) to π*(C19-C21). Other data are given in Table 7. All these cleared that the compound exhibit strong stabilization energy and N-H···O intermolecular interactions influence the crystal packing of ANILAS molecule.

4.5 Ultraviolet – Visible spectral analysis

The calculated electronic absorption spectra were obtained by using TD-DFT method based on B3LYP/6-311G level on the optimized structure. For the title compound, the excitations along with their corresponding wavelengths and assignments were presented in Table 8. In the calculated electronic spectrum (Fig.9) of the title compound, a strong absorption was observed at 218 nm for DMF, 217 nm for water and the calculated gas phase spectrum was observed at 238 nm. The lowering of intensity in the gas phase of UV-visible spectrum is may be due to the solvent effect. Also, this hypochromic effect observed in the UV intensity of gas phase is may be due to the presence of n→π* transition.

4.6 Frontier Molecular Orbital analysis

Molecular Orbital analysis gives the information about the electronic structure of the given molecule. For the present compound, the “Highest Occupied Molecular Orbital” (HOMO) and “Lowest Unoccupied Molecular Orbital” (LUMO) energy is calculated at DFT/B3LYP-6-311G(d,p). The 3D plot of HOMO-LUMO is depicted in Fig.10. HOMO is located completely in arsenate anion whereas LUMO is located completely in anilinium cation. The energy transition implies that electron density transfer from aniline ring to arsenate molecule and the HOMO – LUMO orbitals are anti-bonding orbitals. Similar type of result is observed in melaminium benzoate molecule [43]. HOMO energy is calculated to be -1.1486 *eV* and LUMO energy is calculated to be -6.8390 *eV*. The energy gap is calculated to be = 5.6904 *eV*. The large value of this band gap gives the lesser chemical reactivity and photochemical process with electron transfer [50-52]. In aniline tartrate monohydrate this energy gap value is found to be 3.78 *eV* [12]. By taking into account HOMO and LUMO values, other electronic parameters like global hardness, chemical potential, electrophilicity can be calculated and are listed in Table 9 [52-54].

4.7 Molecular electrostatic potential

The molecular electrostatic potential, v(r), at a given point r (x, y, z) in the vicinity of a molecule, is defined in terms of the interaction energy between the electrical charge generated from the molecule electrons, nuclei and a positive test charge (a proton) located at r. The molecular electrostatic potential (MEP) is related to the electronic density and is a very useful descriptor for determining sites for electrophilic attack and nucleophilic reactions as well as hydrogen-bonding interactions which is indicated by a colour grading [55-57]. Fig.11. shows the 3D plot of molecular electrostatic potential calculated by using the optimized molecular structure at B3LYP/6-31G(d,p) level for ANILAS molecule. Negative electrostatic potential are represented by red colour indicates the electrophilic reactivity; positive electrostatic potential are represented by blue colour indicates nucleophilic reactivity and green colour represents the zero potential. As expected oxygen atoms reflects the negative electro potential and the hydrogen atoms attached to the aniline ring. Amino group of aniline carry the positive charge. These sites give information about the region from where the compound could have non covalent interactions.

4.8 NMR studies

To elucidate the structure, NMR studies have been studied theoretically by using B3LYP/6-311G(d,p) basis set. The ^{1}H and ^{13}C nuclear magnetic resonance (NMR) chemical shifts of ANILAS were calculated using the Gauge-Invariant Atomic Orbital (GIAO) method. **Fig.S1** and **Fig.S2** depicts the theoretically predicted Proton NMR and Carbon NMR spectrum. Table S1 list the calculated chemical shift (GIAO) for ANILAS using B3LYP/ 6-311G(d,p) basis set. The isotropic chemical shifts are generally used as an aid in identification of reactive ionic species. It is well known that substituent position in benzene ring has a major role in determination of structural and electronic properties of the molecules [17]. The amino group attached to the ring produce a downfield shift value of 20.148 δppm (10H) and 20.15 δppm (11H) δppm whereas hydrogen atom (11H) transferred from arsenic anion produces a chemical shift of higher value 28.3779 δppm. All the protons attached to the carbon atoms of aniline ring produces a chemical shift around 24 δppm however ring substituent modifies the basicity of aniline during ion formation tend to reduce the electron density at nitrogen leads to decrease its proton (22H-21.4672 δppm) affinity [58]. Signals of aromatic carbon were computed in the range 46 to 50 δppm and whereas the carbon atom attached to amino group have 59.8735 δppm due to electron density decrease at the ring carbon atom [59]. As no other peaks for carbon and proton are computed, it is clear that the compound has been successfully synthesized and it is a pure material.

4.9 Hirshfeld surface analysis

Hirshfeld analysis of 3D molecular surface and its 2D fingerprint of the compound were created and this study helps to analyse the molecular contributions towards the packing of crystal. It is known that crystal formation depends on the molecular aggregation which can be achieved by knowing the strong hydrogen bonds or other weak non covalent bonds [60]. Figure 12 depicts the entire intercontact of ANILAS. Also, “the various interactions of C-C (3.8%), H-C (14.5%), H-H (34.8%), O-C (0.1%), O-H (45.6%), O-O (1.1%) from the fingerprint are shown in Fig 13. Two sharp spikes pointing down to the plot are typical O–H bonding. This portion contains 45.6% of the total Hirshfeld surface. The next largest strong hydrogen bond interaction portion of 34.8% was contributed by H-H interaction. Also it is seen from Hirshfeld surface area that C-H/H-C intercontact occupies 14.5% and appear as two spikes in the vicinity of de+di ~2.5 Å. Rest of the intermolecular contact are found to be less than 3.8%. All these hydrogen bond and π-πinteractions has reasonable contribution among interacting atoms and are accountable for the packing arrangement and formation of three dimensional networks. The inter contacts of the title compound is clearly seen in 3D form that has been mapped for shape index and curvature as shown in Fig.14. Both shape index and curvature gives similar information. The red and blue triangular spots indicate the hydrogen bonding and π–π stacking in shape index it is indicated by large flat blue region in curved surface [61]. From this analysis we have understood that H-H and O-H bonds followed by C-H bonds have major contribution in the crystal structure.

5. Conclusion

Crystals of ANILAS is built up from mono protonated anilinium cation and deprotonated arsenate anion. Thus the crystal structure of ANILAS is reported in this study is used to understand the role of structure in determining the properties of molecule in key step for the design of new solid materials. ANILAS crystallizes in the monoclinic system with centrosymmetric space group of P21/c. The vibrational spectroscopic analysis elucidates the presence of various functional groups in the aniline and arsenic acid crystalline product. There is a very good agreement between experimental and theoretical frequencies in vibrational spectrum. The strong inter and intramolecular interactions give notable vibrational effect. Further," theoretically obtained powder X-ray diffraction pattern calculates the crystal size as 14.089 μm from Debye Sherrer formula". NBO analysis gives the results about the occurrence f strong stabilization energy and the nature of N-H···O intermolecular interactions that influence the crystal packing of ANILAS molecule. The energy gap of 5.6904 eV gives the lesser chemical reactivity and photochemical process with electron transfer. The structure is further elucidated by ^{1}H and ^{13}C NMR spectrum using Gauge-Invariant Atomic Orbital (GIAO) method. Electrostatic potential map well establishes the possible nucleophilic and electrophilic reactions of the compound. The Hirshfeld surface analysis with finger prints and electrostatic potential map shed more light on the percentage of intermolecular contacts and distribution of electrostatic potential of the title compound.

Supplementary material

Full crystallographic data (cif file) relating to the crystal structure has been deposited with Cambridge Crystallographic Data centre as CCDC 1875920. Copies of this information can be obtained free of charge from the Cambridge Crystallographic Data Centre, 12 Union Road, Cambridge CB2 1Ez. UK (Tel: +44(0) 1223 762911;

Email: deposit@ccdc.cam.ac.uk:http://www.ccdc.cam.ac.uk)

Credit author statement

1. N.Kanagathara – Concept and design of the work, Drafting the article – final approval of the version
2. F.Mary Anjalin – Literature survey, data collection
3. V.Ragavendran – DFT- Gaussian 09 computation
4. D.Dhanasekaran – critical revision of the article – proof reading - intrepretation
5. R.Usha – critical revision of the article – NMR part
6. R.Gowri Shankar Rao – Interpretation of the results
7. M.K.Marchewka – proof checking – manuscript correction

Declaration of interests

The authors declare that they have no known competing financial interests or personal relationships that could have appeared to influence the work reported in this paper.

References

[1] Poul Erik Hansen, Jens Spanget-Larsen, On prediction of OH stretching frequencies in intramolecularly hydrogen bonded systems, J.Mol.Struc. 101827(2012)8-13.

[2] R.Thakuria, B.Sarma, A.Nangia, 7.03-Hydrogen bonding in molecular crystals, Comprehensive supramolecular chemistry II, (2017)25-48.

[3] Anamika Sharma, Vineet Gupta, Rashmi Mishra, Poonam Tandon, Shiro Maeda, Koki-Kunimoto,Study of vibrational spectra and molecular structure of intermolecular hydrogen bonded 2-thiohydantoin using Density Functional Theory, J.Mol.Struc. 1004(1) (2011) 237-247.

[4] S. Thirunarayanan, V. Arjunan, M. K. Marchewka, S. Mohan, Structure, vibrations and quantum chemical investigations of hydrogen bonded complex of bis(1–hydroxy–2–methylpropan–2–aminium)selenate, J.Mol.Struc. 113415 (2017) 6-16.

[5] V.Siva, S.Suresh Kumar, M.Suresh, M.Raja, S.Athimoolam, S.Asath Bahadur, N-H···O hydrogen bonded novel nonlinear optical semiorganic crystal (4-methoxyanilinium trifluoroacetate) studied through theoretical and experimental methods, J.Mol.Struc. 1133 (2017) 163-171.

[6] S.Kumar, A.Nanda, Pharmaceutical Cocrystals: An Overview, Indian J Pharm Sci. 79(6) (2017) 858-871.

[7] S. Shaji, S.M. Eappen, T.M.A. Rasheed, K.P. R Nair, NIR vibrational overtone spectra of N-methylaniline, N,N-dimethylaniline and N,N-diethylaniline—a conformational structural analysis using local mode model, Spectrochim. Acta A 60 (2004) 351–355.

[8] M. Arivazhagan, V.P.Subhasini, A.Austine, Vibrational spectroscopic, first-order hyperpolarizability and HOMO, LUMO studies of 4-chloro-2-(trifluoromethyl) aniline based on DFT calculations, Spectrochim. Acta A 86 (2012) 205-213.

[9] E..Kavitha, N.Sundaraganesan, S.Sebastian, Molecular structure, vibrational spectroscopic and HOMO-LUMO studies of 4-nitroaniline by density functional method, Indian J. Phys. 48 (2010) 20-30.

[10] R.P.Singh, R.N.Singh, Vibrational spectra of 2,3 and 2,6 dichloro anilines, Pramana J. Phys. 30(3) (1988) 217-223.

[11] M.K.Marchewka, S.Debrus, M.Drozd, J.Baran, A.J.Barnes, D.Xue, H.Ratajczak, Vibrational spectra, phase transition and nonlinear optical properties of anilinium perchlorate molecular – ionic solid, Polish J.Chem., 77 (2003) 1625-1636.

[12] N.Kanagathara, M.K.Marchewka, G.Anbalagan, A.Ben Ahmed, H.Feki, Molecular Structure, vibrational spectra and first order hyper polarizabikity studies on anilinium L-tartrate monohydrate, J Optoelectron Adv M., 19 (2017) 251 – 265.

[13] M.Targema, O.Nelson, Obi-Egbedi, D.Moriam, C.Adeoye, Molecular structure and solvent effects on the dipole moments and polarizabilities of some aniline derivatives, Comput. Theor. Chem. 1012 (2013) 47–53.

[14] F.MaryAnjalin, N.Kanagathara, M.K.Marchewka, T.Srinivasan, Structural, spectroscopic and Hirshfeld analysis of anilinium malonate, Asian J. Chem. 31 (2019) 860-872

[15] M.Sardari, F.K.Fotooh, M.R.Nateghi, A DFT study of the structural and electronic properties of periodic forms of aniline and pyrrole polymers and aniline–pyrrole copolymer. J Mol Model., 24 (2018) 148-158.

[16] M. Przybylek, J.Gaca, Reaction of aniline with ammonium persulphate and concentrated hydrochloric acid: Experimental and DFT studies, Chem. Pap., 66 (7) (2012) 699–708.

[17] M. Karabacak, M. Kurt, M.Çınar, Ali Çoruh, Experimental (UV, NMR, IR and Raman) and theoretical spectroscopic properties of 2-chloro-6-methylaniline, Mol. Phys., 107:3 (2009) 253-264.

[18] H. Tanak, K. Pawlus, M. K. Marchewka, A. Pietraszko, Structural, vibrational and theoretical studies of anilinium trichloroacetate: New hydrogen bonded molecular crystal with nonlinear optical properties, Spectrochim. Acta A, 118 (2014) 82-93.

[19] M. K. Marchewka, A. Pietraszko, Structural and vibrational studies of anilinium nitrate, J Phys. Chem. Solids, 66 (2005) 1039-1048.

[20] G.Anbalagan, M.K.Marchewka, K.Pawlus, N.Kanagathara, Crystal Structure and vibrational spectra of melaminium arsenate, J.Mol. Struc. 1079 (2015) 407-413.

[21] M.K. Marchewka, S. Debrus, H. Ratajczak, Vibrational Spectra and Second Harmonic Generation in Molecular Complexes of L-Lysine with L-Tartaric, D,L-Malic, Acetic, Arsenous, and Fumaric Acids, Cryst. Growth Des., 3 (2003) 587-592.

[22] Kuma Diffraction, KM4/CCD Users' Guide, Version 1.169 (Release April, 2000), Wroclaw, Poland, 2000.

[23] G.M.Sheldrick, X.L.SHEL, Program for Crystal Structure Refinement, University of Gottingen, Germany, 1993.

[24] G.M.Sheldrick, A short history of SHELX, ActaCryst. A 64 (2008) 112-122.

[25] M.J.Frisch, G.W. Trucks, H.B.Schlegel, G.E.Scuseria, M.A.Robb, J.R. Cheeseman, G.Scalmani, V.Barone, B.Mennucci, G.A.Petersson, Gaussian 09, Revision D.01; Gaussian, Inc.: Wallingford, CT, 2010.

[26] E.D.Glenening, A.E.Reed, J.E.Carpenter, F. Weinhold, J.A. Bohmann, C.M. Morales, NBO version 5.0, Theoretical Chemistry Institute University of Wisconsin Madison; 2001.

[27] J.B.Foresman, A.Frisch, Exploring Chemistry with electronic structure methods, Gaussian Inc. Pittsburgh, 1996.

[28] C.F. Macrae, P.R. Edgington, P. Mccabe, E. Pidcock, G.P. Shields, R. Taylor, J.V.D.Streek, P.A.Wood, **Mercury**: Visualization and analysis of crystal structures J Appl.Cryst.39 (2006) 453–457.

[29] M. J. Turner, J. J. McKinnon, S. K. Wolff, D. J. Grimwood, P. R. Spackman, D. Jayatilaka and M. A. Spackman, Crystal Explorer 17 University of Western Australia 2017.

[30] S. K. Wolff, D. J. Greenwood, J. J. McKinnon, M. J. Turner, D. Jayatilaka, M. A. Spackman., Crystal Explorer, Version 3.1 2012.

[31] M.A.Spackman, J.J.McKinnon, D.Jayatilaka, Electrostatic potentials mapped on Hirshfeld surfaces provide direct insight into intermolecular interactions in crystals, Cryst. Eng. Comm. 10 (2008) 377-388.

[32] M. A. Spackman, J. J. McKinnon, Fingerprinting intermolecular interactions in molecular crystals, Cryst. Eng. Comm. 4 (2002) 378–392.

[33] M. V. Castillo, R.A. Rudyk , L.Davies , S. A.Brandan, Analysis of the structure and the FT-IR and Raman spectra of 2-(4-nitrophenyl)-4H-3,1-benzoxazin-4-one. Comparisons with the chlorinated and methylated derivatives, J. Mol. Struc., 1140 (2017) 2-11.

[34] P.M.Wojciechowski, W.Zierkiewicz, D.Michalskaa, P.Hobza, Electronic structures, vibrational spectra, and revised assignment of aniline and its radical cation: Theoretical study, J. Chem. Phys. 118 (2003) 10900-10911.

[35] M.Rademeyer, Anilinium nitrate, Acta Cryst. E 60 (2004) o958-o960.

[36] W. Smirani, A. Ben Slimane and M. Rzaigui, Crystal structure of 4-methylanilinium dihydrogenphosphate, (*p*-CH3C6H4NH3)(H2PO4), Z. Kristallogr. NCS 219 (2004) 189–190.

[37] J. A. PaixaÄo, A.MatosBeja, M.Ramos Silva, J. Martin-Gil, Two anilinium salts: anilinium hydro-genphosphite and anilinium hydrogen-oxalate hemihydrate, Acta Cryst. C56 (2000) 1132-1135.

[38] G.J.Perpeatuo, J.Janczak, Anilinium monohydrogen DL-malate, Acta Cryst. C59 (2003) o709-o711.

[39] R. M. Siverstein, F. X. Webster, Spectrometric Identification of Organic Compounds, Sixth Ed., Wiley Chapter 3 (1998) 102.

[40] N.Sheppard, University of East Anglia, Norwich, UK, The historical development of experimental techniques in vibrational spectroscopy, John Wiley & Sons Ltd, 2002, 1-4484.

[41] J.Swaminathan, M.Ramalingam, V.Sethuraman, N.Sundaraganesan, S.Sebastian, Vibrational spectroscopic studies and DFT calculations of 4-aminoantipyrine, Spectrochim. Acta A 73 (2009) 593-600.

[42] M.Drozd, M.K.Marchewka , The structure, vibrational spectra and nonlinear optical properties of neutral melamine and singly, doubly and triply protonated melaminiumcations - Theoretical studies, J. Mol. Struc. Theochem. 716 (2005) 175-192.

[43] N.Kanagathara, M.K.Marchewka, M.Drozd, P.R.Rajakumar, S.Gunasekaran, G.Anbalagan, Structural and vibrational spectroscopic studies on charge transfer and ionic hydrogen bonding interactions of melaminium benzoate dihydrate, Spectrochim. Acta A 145 (2015) 395-409.

[44] D.N.Sathyanarayana, Vibrational Spectroscopy, Theory and Applications New Age International (P) limited publishers, New Delhi 1996.

[45] R.L. Frost , A.Lopez , Y.Xi, C.Lana, L.Souza, R.Scholz, J.Sejkora , J.Cejka, A vibrational spectroscopic study of the arsenate minerals cobalt koritnigite and koritnigite, Spectrochim. Acta A, 125 (2014) 313–318.

[46] L.D.Pettit, D.Turner, The infrared spectra of organo arsenic compounds, Spectrochim. Acta A, 24A (1908) 999-1006.

[47] F.K.Vansant, B.J.Van Der Veken, H.O.Dessryn, Vibrational Analysis of Arsenic acid and its anions, J. Mol. Struc.15 (1973) 425-437.

[48] M.Khalid, A.Ali, M.Adeel, Z.U.Din, M.N.Tahir, E.Rodrigues-Filho, J.Iqbal, M.U.Khan, Facile preparation, characterization, SC-XRD and DFT/DTDFT study of diversely functionalized unsymmetrical bis-aryl-*α, β*-unsaturated ketone derivatives, J. Mol. Struc.1206 (2020) 127755.

[49] S.Tariq, M.Khalid, A. Rauf Raza, S.L. Rubab, S.F. de A. Morais, M.U.Khan, M.N.Tahir, A.A.C.Braga, Experimental and computational investigations of new indole derivatives: A combined spectroscopic, SC-XRD, DFT/TD-DFT and QTAIM analysis, J.Mol.Struc, 1207 (2020) 127803.

[50] E.Khan, M.Khalid, Z.Gul, A.Shahzad, M.N.Tahir, H.M.Asif, S.Asim, A.AC.Braga, Molecular structure of 1,4-bis(substituted-carbonyl)benzene: A combined experimental and theoretical approach, J.Mol.Struc. 1205 (2020) 127633.

[51] K.Fukui, Theory of Orientation and Stereoselection, Reactivity and Structure, Concepts in Organic Chemistry, Springer, Berlin 1975.

[52] C.Theivarasu, R.Murugesan, Natural Bond Orbital (NBO) Population analysis of an energetic molecule 1-Phenyl-2-nitroguanidine, Ind.J.Chem.Sci. 14(4) (2016) 2019-2020.

[53] R.G. Parr, L.V. Szentpaly, S.J. Liu, Electrophilicity Index, Am. Chem. Soc. 121 (1999) 1922 –1924.

[54] H.Abbas, M.Shkir, S.Alfaify, Density functional study of spectroscopy, electronic structure, linear and nonlinear optical properties of L-proline lithium chloride and L-proline lithium bromide monohydrate: For laser applications. Asian J. Chem., 12 (2019) 2336-2346.

[55] S. Sebastin, N. Sundaraganesan, The spectroscopic (FT-IR, FT-IR gas phase, FT-Raman and UV) and NBO analysis of 4-Hydroxypiperidine by density functional method, Spectrochim. Acta A 75 (2010) 941–952.

[56] E. Scrocco, J. Tomasi, The electrostatic molecular potential as a tool for the interpretation of molecular properties, Adv. Quantum Chem. (1979) 111–115.

[57] S.Tariq, A. Rauf Raza, M.Khalid, S.L. Rubab, M.U.Khan, A.Ali, M.N.Tahir, A.A.C.Braga, Synthesis and structural analysis of novel indole derivatives by XRD, spectroscopic and DFT studies, J.Mol.Struc., 1203 (2020) 127438.

[58] T. Axenrod, P. S. Pregosin, M. J. Wieder, E. D. Becker, R. B. Bradley, G. W. A. Milne, Nitrogen- 15 Nuclear Magnetic Resonance Spectroscopy. Substituent Effects on "N-H Coupling Constants and Nitrogen Chemical Shifts in Aniline Derivatives, J. Am. Chem. Soc., 93:24 (1971) 6536-6541.

[59] Chien-Chung Han, R. Balakumar, D. Thirumalai, Ming-Tsu Chung, The different electronic natures displayed by the alkylthio groups in simple and higher conjugated aniline systems, Org. Biomol. Chem., 4 (2006) 3511–3516.

[60] G. R. Desiraju, T. Steiner, The Weak Hydrogen Bond in Structural Chemistry and Biology. [éd.] Oxford University Press. Oxford,:s.n., 1999.

[61] A.Ali, M.Khalid, S.Abid, J.Iqbal, M.N.Tahir, A.RaufRaza, J.Zukerman, M.W.Paixao, Facile synthesis, crystal growth, characterization and computational study of new pyridine-based halogenated hydrazones: Unveiling the stabilization behaviour in terms of non covalent interactions, Appl. Organo metal. Chem. 34 (2019) e5399 , 1-15.

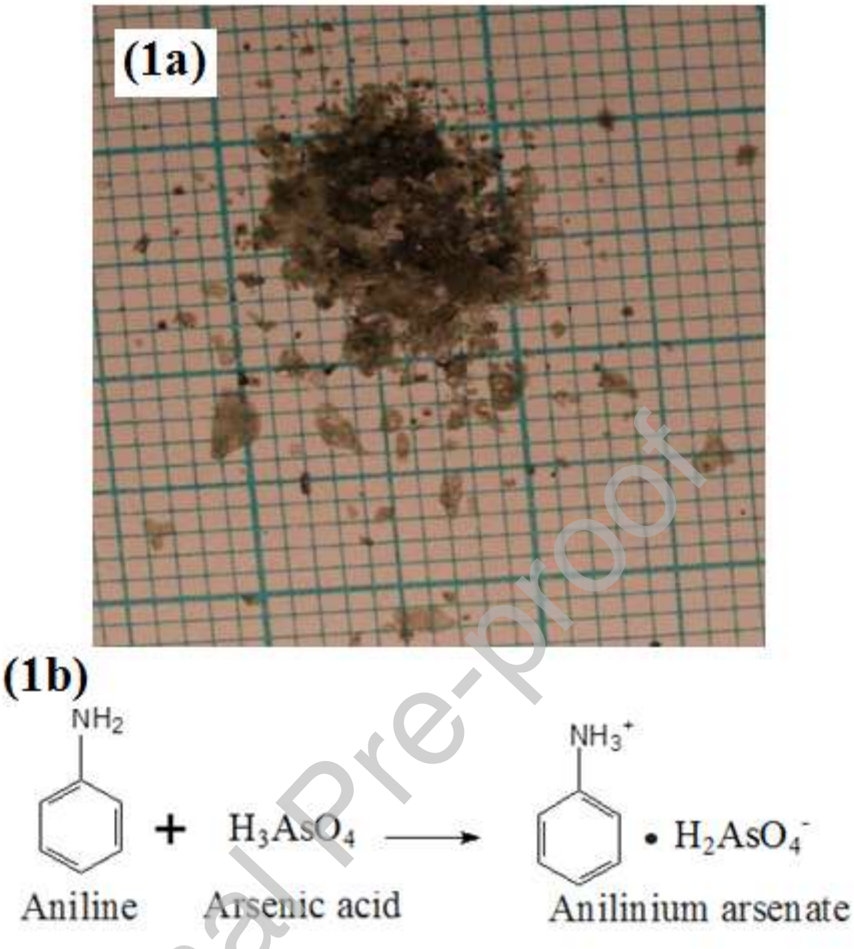

Fig.1a and 1b Photograph and reaction scheme of ANILAS

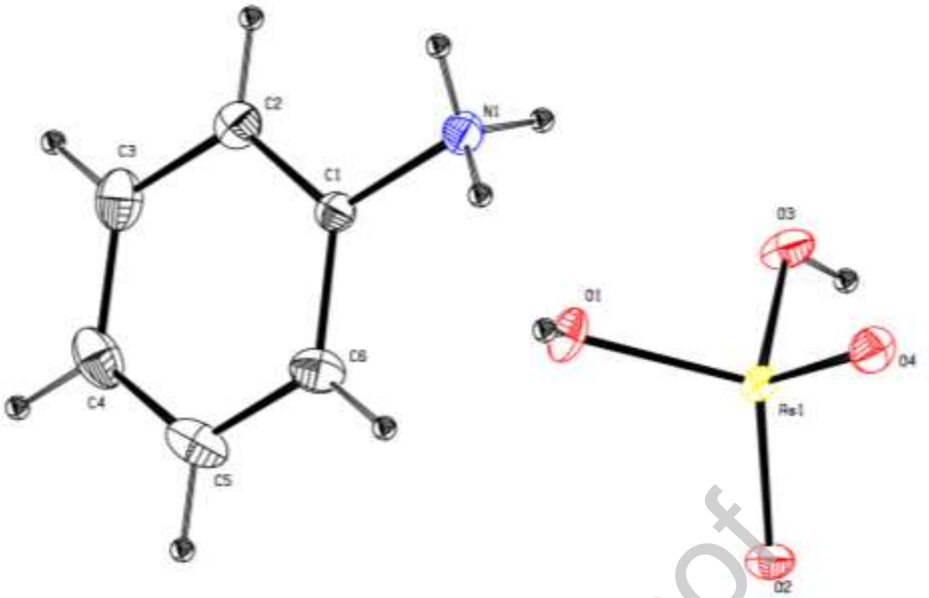

Fig.2 ORTEP plot of ANILAS with the atom numbering scheme. Displacement ellipsoids are drawn at 30% probability level

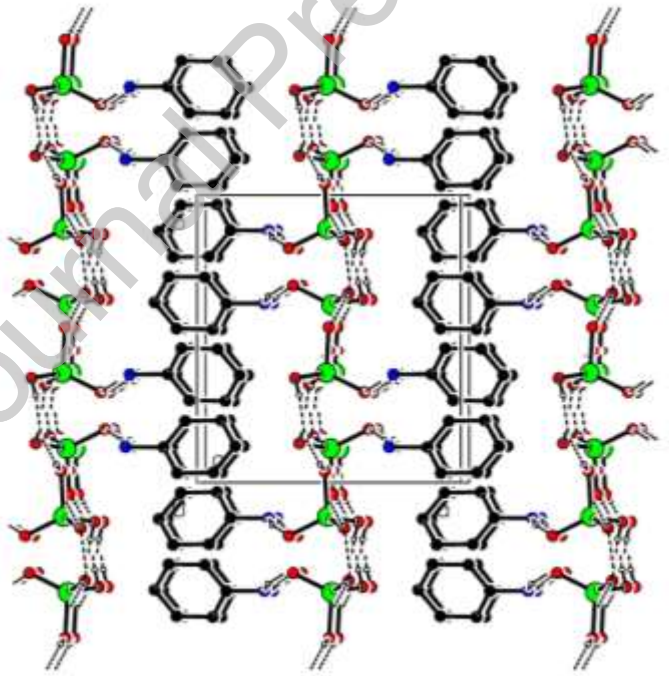

Fig.3 The molecular packing of ANILAS forming two dimensional networks viewed along c axis

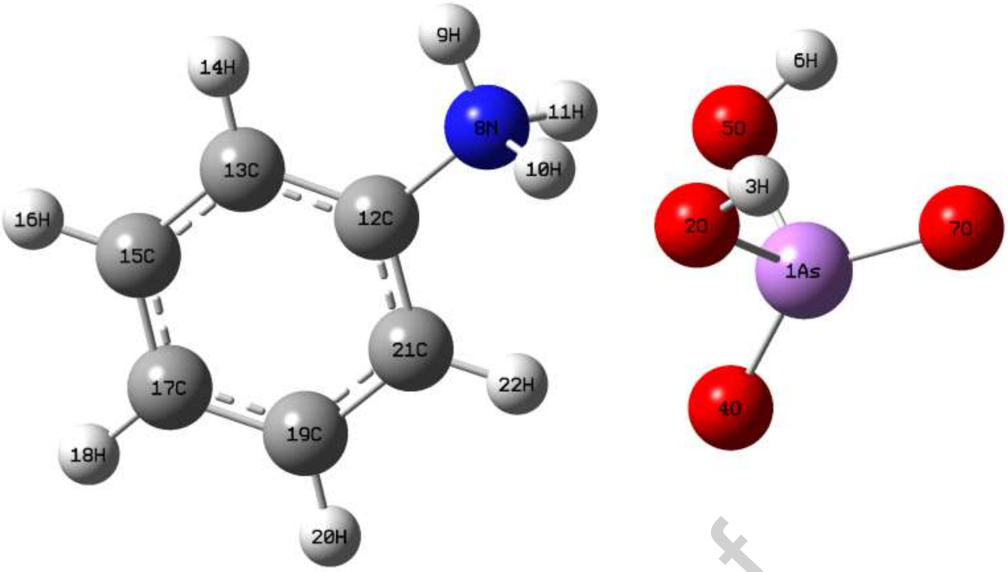

Fig.4 Optimized structure of ANILAS

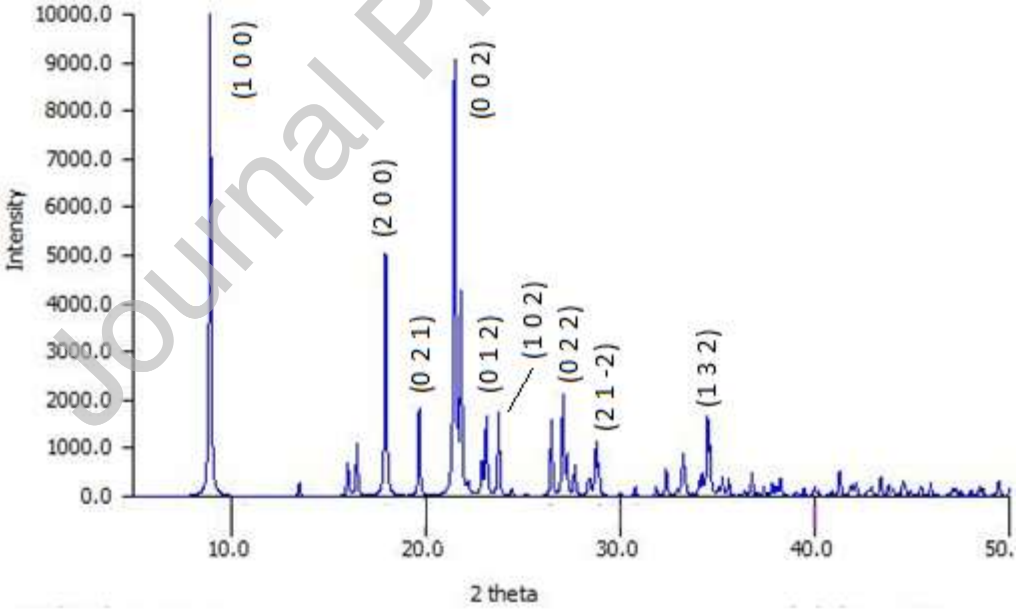

Fig.5 Simulated powder X-ray diffraction pattern of ANILAS

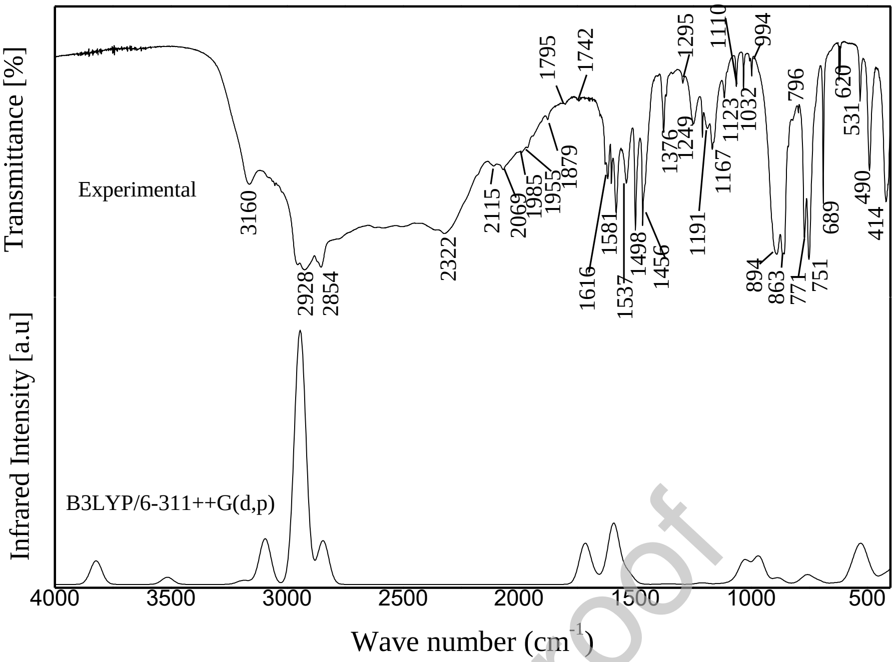

Fig.6 Experimental and theoretical FT-IR spectra of ANILAS

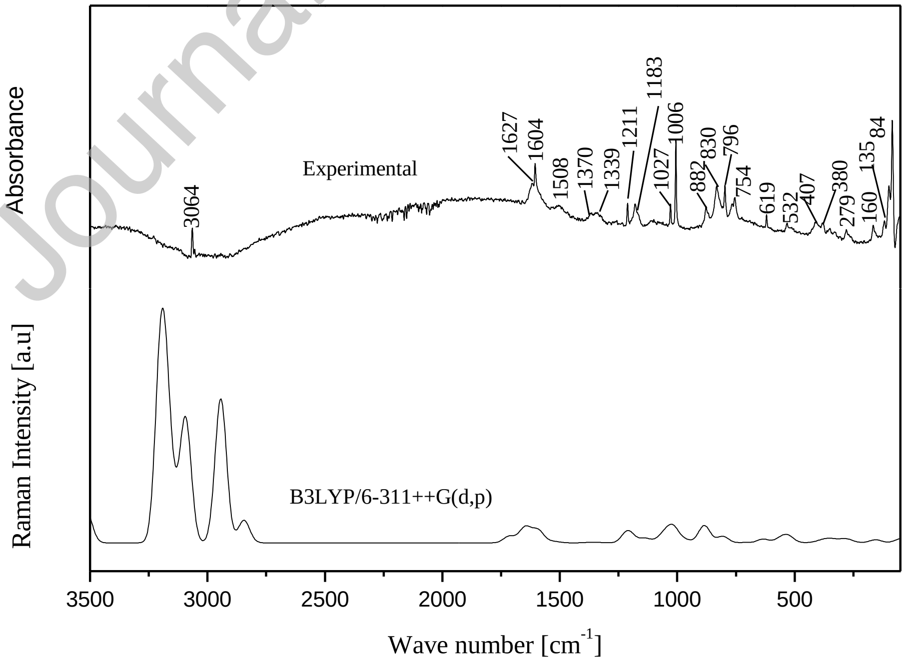

Fig.7 Experimental and theoretical FT-Raman spectra of ANILAS

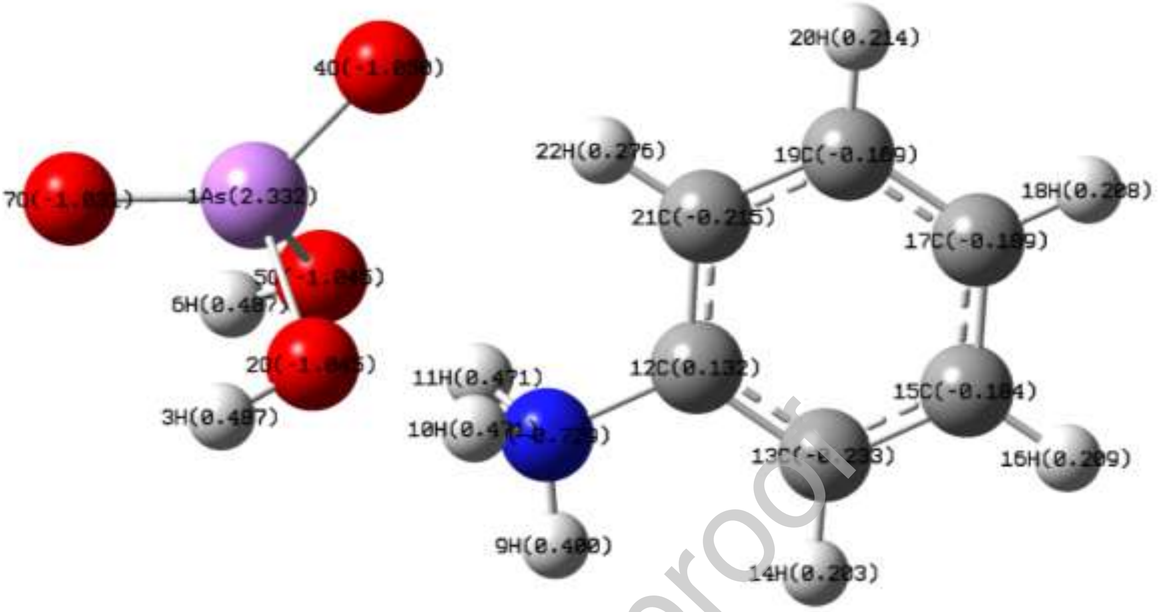

Fig.8 NBO of ANILAS

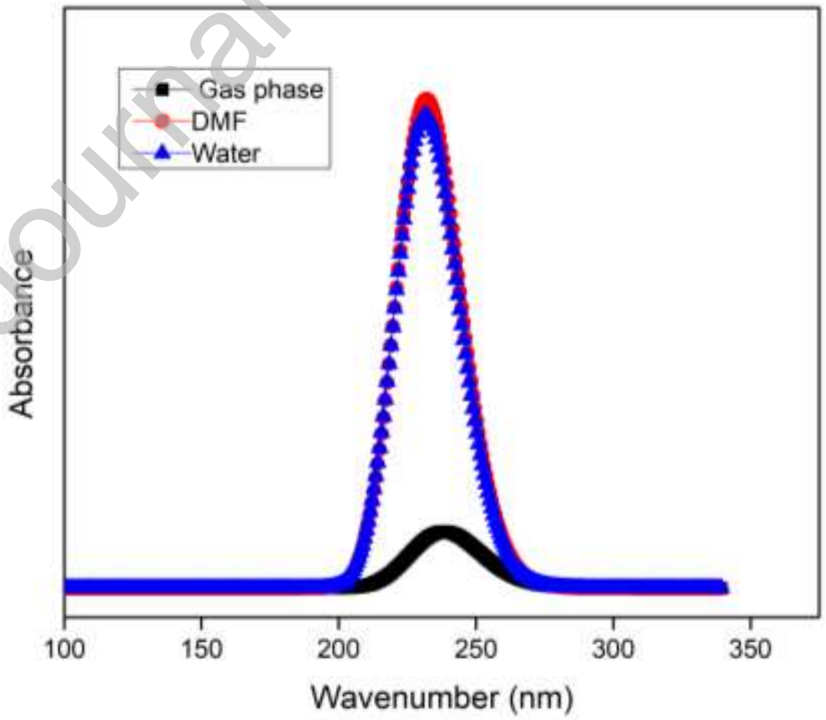

Fig.9 UV-Vis spectrum of ANILAS calculated at B3LYP/6-311G(d,p)

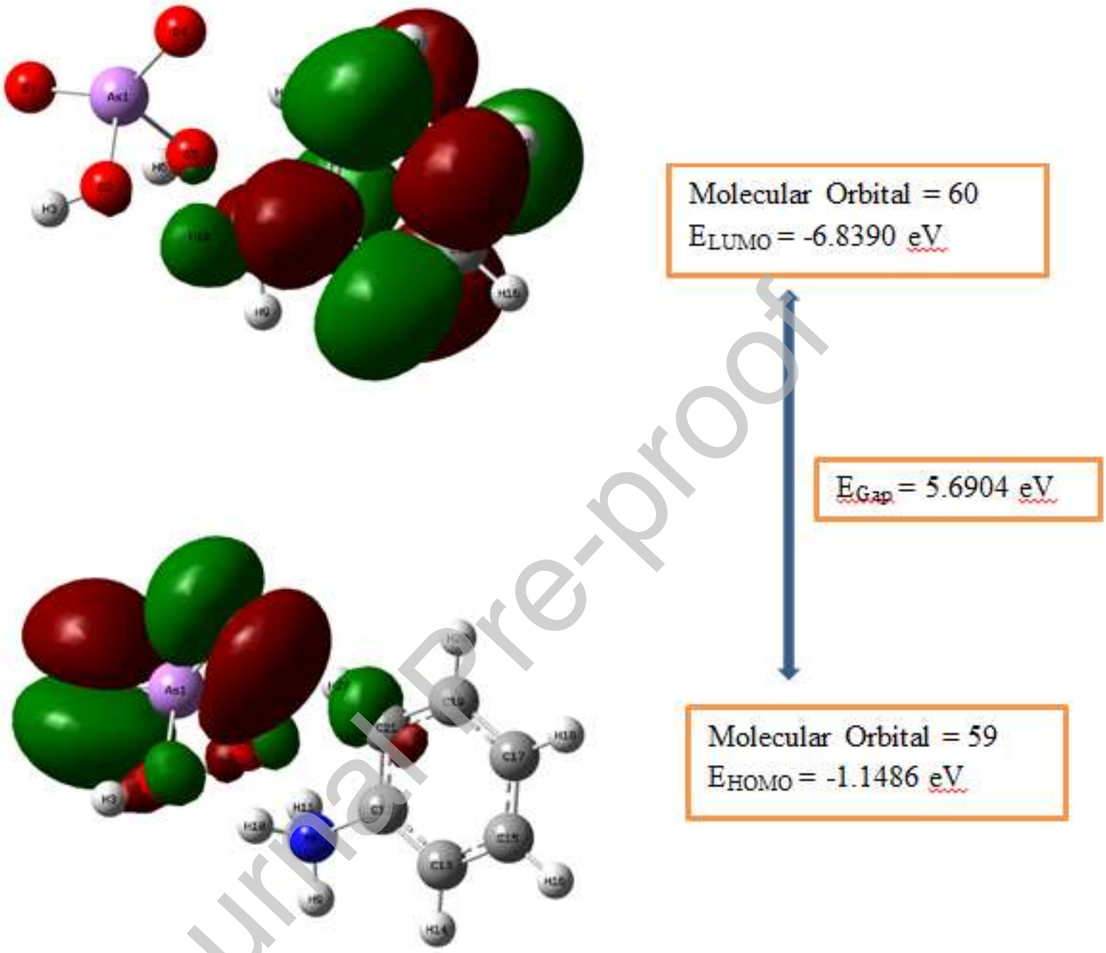

Fig. 10 HOMO and LUMO plot of ANILAS

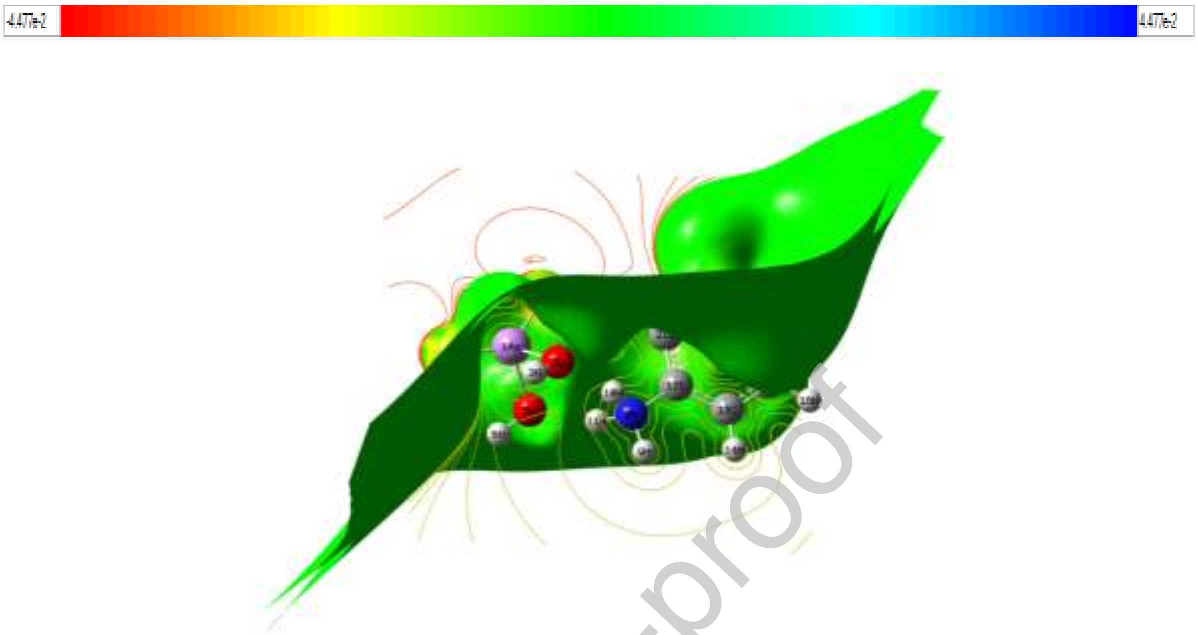

Fig.11 Molecular electrostatic potential map

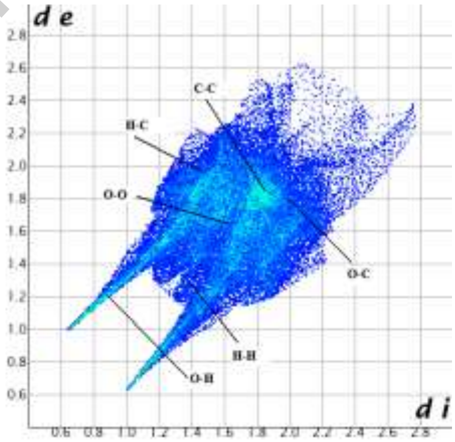

Fig.12 Fingerprint of ANILAS (100%)

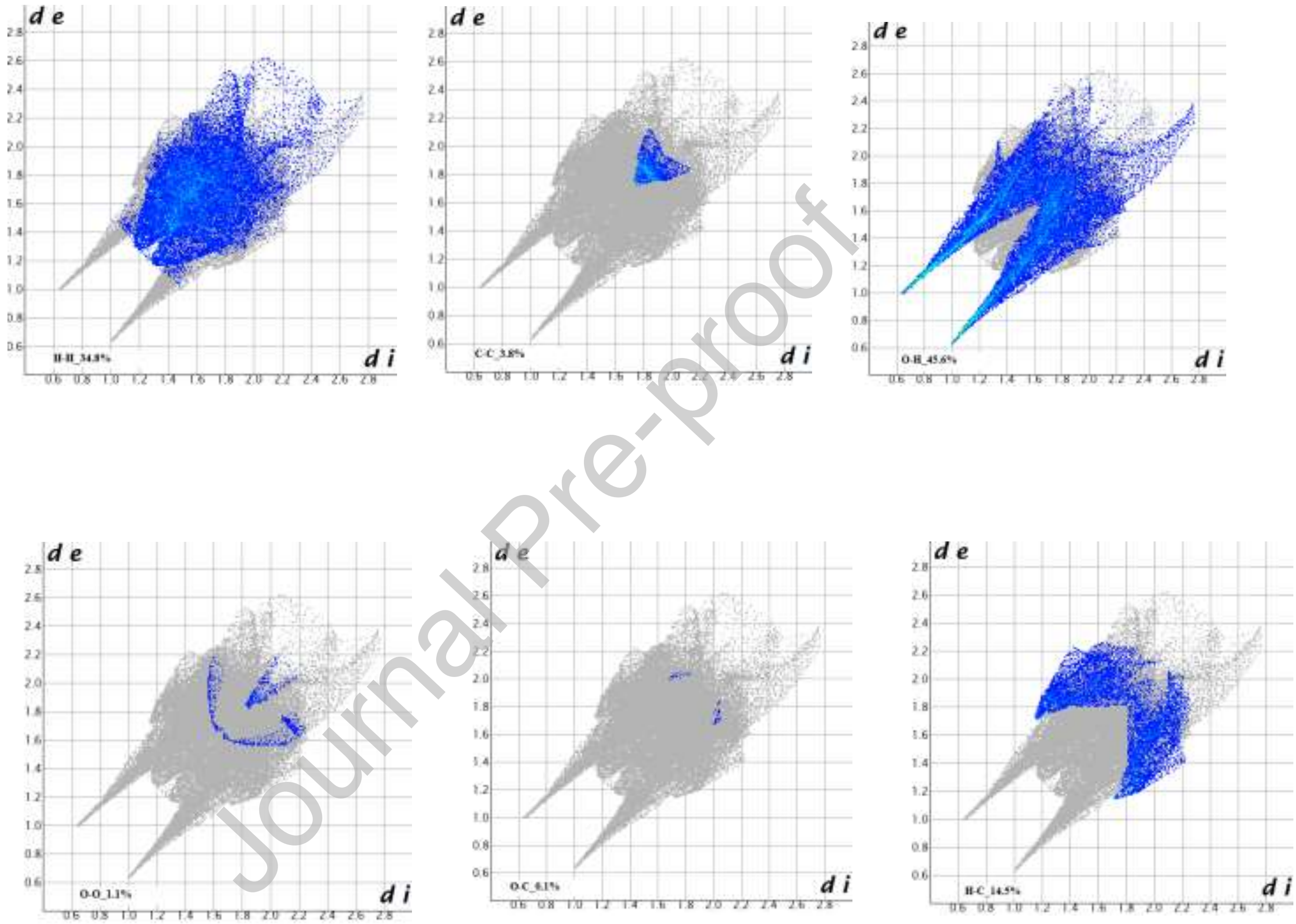

Fig.13 Relative contributions to the percentage of Hirshfeld surface areas C-C (3.8%), H-C (14.5%), H-H (34.8%), O-C (0.1%), O-H (45.6%), O-O (1.1%) of intermolecular contacts in ANILAS

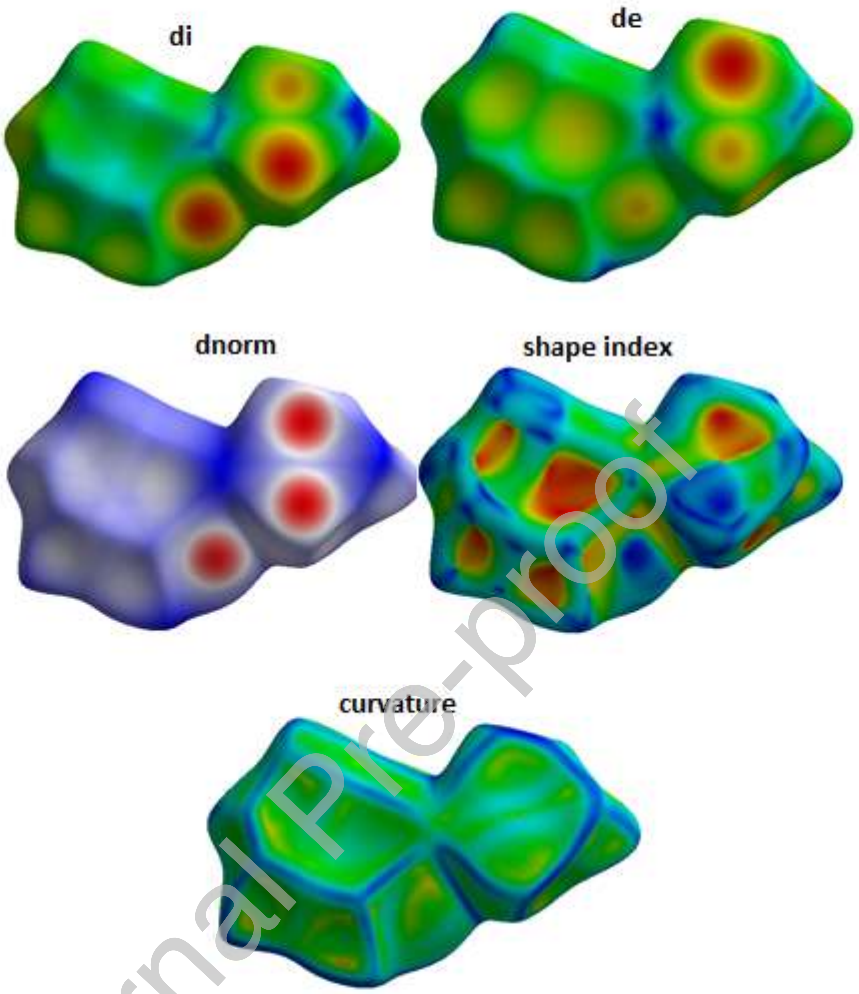

Fig.14. Hirshfeld surface analysis di, de, dnorm, shape index and curvedness of ANILAS

Table 1. Crystal data and structure refinement for ANILAS

Empirical formula	C6 H10 As N O4
Formula weight (g mol^{-1})	235.07
Temperature (K)	293(2)
Wavelength (A)	0.71073 Å
Crystal system	Monoclinic
Space group	P2(1)/n
a	9.872(2))Å
b	10.769(2)Å
c	8.223(2)Å
α	90^{o}
β	92.23(3)^{o}
γ	90^{o}
V	873.5(3) (Å)^{3}
Z	4
D $_{calc}$(Mg m^{-3})	1.787
Absorption coefficient (mm^{-1})	3.867
F(000)	472
Crystal size (mm)	0.21 x 0.13x 0.12
Theta range for data collection (^{o})	3.69-29.54
Index ranges	h=-13→13; k=-14→14; l=-10→11
Completeness to θ	100%
Refinement method	Full-matrix least squares on F2
Data/restraints/parameters	2289/0/125;
R indexes [I>=2<sigma> (I)]	0.0341 ; wR-0.0852
Final R indexes [all data]	0.0391; wR-0.0876
Goodness of fit on F^{2}	1.008
Extinction coefficient	0.087(4)
Largest differences peak and hole (e.Å^{-3})	0.866 and -1.030

Table 2. Selected experimental and calculated [B3LYP/6-311G(d,p)] bond distances (Å) and bond angles (°)

Atom	Bond distance(Å)		Atom	Bond distance(Å)	
	Expt.	**Calculated**		**Expt.**	**Calculated**
As1-O4	1.655	1.6324	C3-H3	0.930	1.0834
As1-O2	1.658	1.6337	C4-C5	1.382	1.3941
As1-O3	1.713	1.8705	C4-H4	0.930	1.0837
As1-O1	1.723	1.8705	C5-C6	1.390	1.3983
O1-H111	0.85	0.965	C5-H5	0.930	1.0834
O3-H311	0.73	0.965	C6-H6	0.930	1.0903
C1-C6	1.377	1.3907	N1-C1	1.462	1.4716
C1-C2	1.377	1.3893	N1-H11	0.81	1.0578
C2-C3	1.387	1.3931	N1-H12	0.85	1.0578
C2-H2	0.930	1.0857	N1-H13	0.93	1.0185
C3-C4	1.375	1.3926			

Atom	Bond angle (°)		Atom	Bond angle (°)	
	Expt.	**Calculated**		**Expt.**	**Calculated**
O4-As1-O2	115.85	134.73	C1-N1-H11	111	111.32
O4-As1-O3	111.88	106.23	C1-N1-H12	102	114.06
O2-As1-O3	109.05	107.04	H11-N1-H12	114	114.05
O4-As1-O1	111.10	107.05	C1-N1-H13	106.4	111.32
O2-As1-O1	110.73	104.15	H11-N1-H13	105	99.65
O3-As1-O1	96.57	94.18	H12-N1-H13	117	108.52
As1-O1-H111	114	107.05	C6-C1-C2	121.6	122.29
As1-O3-H311	108	107.05	C3-C4-C5	119.7	120.12
C6-C1-N1	119.5	119.12	C3-C4-H4	120.1	119.87

C2-C1-N1	118.8	118.58	C5-C4-H4	120.1	120.01
C1-C2-C3	119.3	118.95	C4-C5-C6	120.8	120.84
C1-C2-H2	120.4	120.81	C4-C5-H5	119.6	120.18
C3-C2- H2	120.4	120.24	C6-C5-H5	119.6	118.98
C4-C3-C2	120.3	119.87	C1-C6-C5	118.4	117.92
C4-C3-H3	119.9	120.44	C1-C6-H6	120.8	120.64
C2-C3-H3	119.9	119.69	C5-C6-H6	120.8	121.44

Table 3.Hydrogen bond symmetry

D-H···A	**D···H**	**H···A**	**D···A**	**D-H···A**
N1-H12… O1	0.81(4)	1.95(4)	2.750(3)	169(3)
N1-H11… O4	0.81(4)	1.95(4)	2.750(3)	169(3)
N1-H13… O4	0.93(3)	1.82(3)	2.736(3)	170(3)
O1-H111… O2	0.85(4)	1.60(4)	2.380(2)	150(3)
O3- H311… O2	0.73(4)	1.88(4)	2.594(2)	166(4)

Symmetry codes: i) 1-x,1/2+y,1/2-z; ii) 1-x,2-y,-z iii) 1-x,2-y,1-z iv) x,3/2-y,-1/2+z

Table 4. Atomic displacement parameters (Å^2)

Atom	U11	U22	U33	U23	U13	U12
As1	0.02873(17)	0.02258(16)	0.02019(16)	0.00073(7)	0.00238(9)	0.00090(7)
O1	0.0417(9)	0.0369(9)	0.0294(8)	0.0106(7)	0.0141(7)	0.0116(7)
O2	0.0484(9)	0.0273(8)	0.0261(7)	0.0022(6)	0.0013(7)	0.0085(7)
O3	0.0648(12)	0.0247(8)	0.0249(9)	0.0010(7)	0.0050(8)	0.0030(7)
O4	0.0314(7)	0.0427(9)	0.0361(9)	0.0028(8)	0.0016(7)	0.0093(7)
N1	0.0301(10)	0.0371(12)	0.0293(10)	0.0003(8)	0.0018(8)	0.0013(7)
C1	0.0317(11)	0.0297(11)	0.0225(10)	-0.0034(8)	0.0002(9)	0.0023(8)
C2	0.0422(12)	0.0392(13)	0.0390(13)	0.0004(11)	0.0033(11)	0.0012(11)
C3	0.0407(13)	0.0527(16)	0.0538(16)	-0.0120(14)	0.0079(12)	-0.0109(12)
C4	0.0320(13)	0.0605(19)	0.0609(19)	-0.0192(14)	-0.0096(13)	0.0031(11)
C5	0.0546(16)	0.0486(16)	0.062(2)	-0.0010(15)	-0.0158(16)	0.0155(14)
C6	0.0494(14)	0.0348(13)	0.0474(16)	0.0032(11)	-0.0052(12)	0.0026(11)

Table 5. Fractional atomic coordinates and isotropic or equivalent isotropic displacement parameters (Å^2)

Atom	x	y	z	U iso or equi
As1	0.50315(2)	0.881607(18)	0.28611(2)	0.02380(13)
O1	0.61623(19)	0.86333(16)	0.1334(2)	0.0357(4)
H111	0.598(3)	0.804(3)	0.068(4)	0.054
O2	0.57366(17)	0.84142(15)	0.46471(19)	0.0340(4)
O3	0.4932(2)	1.04026(16)	0.2756(2)	0.0380(4)
H311	0.478(4)	1.063(3)	0.356(5)	0.057
O4	0.35612(16)	0.81487(17)	0.2371(2)	0.0368(4)
N1	0.7309(2)	1.1237(2)	0.0742(3)	0.0322(4)
H11	0.714(3)	1.148(3)	-0.017(5)	0.048
H12	0.710(3)	1.048(3)	0.090(4)	0.048
H13	0.694(3)	1.182(3)	0.142(4)	0.048
C1	0.8768(2)	1.12283(18)	0.1126(3)	0.0280(5)
C2	0.9561(3)	1.2142(2)	0.0480(3)	0.0401(5)
H2	0.9176	1.2740	-0.0210	0.048
C3	1.0940(3)	1.2161(3)	0.0872(4)	0.0489(7)
H3	1.1482	1.2781	0.0452	0.059
C4	1.1509(3)	1.1267(3)	0.1877(4)	0.0514(8)
H4	1.2436	1.1276	0.2130	0.062
C5	1.0698(3)	1.0354(3)	0.2511(4)	0.0557(8)
H5	1.1085	0.9750	0.3190	0.067
C6	0.9312(3)	1.0328(2)	0.2145(4)	0.0441(6)
H6	0.8765	0.9717	0.2578	0.053

Table 6.Wavenumbers (cm^{-1}) and relative intensities of observed and calculated Fourier Infrared and Raman spectra of ANILAS

Experimental frequencies		**Calculated frequencies at DFT/B3LYP/6-311G(d,p)**				**Band assignment Description**
FT-IR cm^{-1}	**FT Raman cm^{-1}**	**unscaled**	**scaled**	**IR Intensity**	**Raman activity**	
		3823	3700	92.581	150.843	O-H asymmetric vibration of Arsenate anion
		3821	3698	47.663	71.629	O-H asymmetric vibration of Arsenate anion
	3390m	3515	3402	42.382	55.345	NH_3 asymmetric stretching vibration
3160s		3198	3095	10.301	267.384	C-H asymmetric stretching
	3064m	3190	3088	7.986	66.926	C-H asymmetric stretching
	3056m	3176	3074	2.937	82.464	C-H symmetric stretching
3056s		3156	3055	8.674	70.631	C-H symmetric stretching
2958s		3093	2994	270.937	221.152	C-H symmetric stretching
2854s		2943	2848	1506.302	255.219	N-H asymmetric stretching (N-H⋯O)
2773s		2844	2753	259.716	39.937	N-H asymmetric stretching (N-H⋯O)
1692w		1715	1660	240.783	11.501	NH_3 in-plane bending vibration
1628m	1627w	1666	1612	28.583	3.586	NH_3 in-plane bending vibration
1603s	1604m	1651	1598	3.003	7.539	C-C stretching ; N-H stretching
1592s	1581s	1642	1590	7.696	18.085	C-C stretching ; N-H stretching
1537s		1592	1541	357.746	22.127	C-C stretching ; N-H stretching
1498vs	1508w	1534	1485	70.451	2.620	C-H bending /C-C stretching vibration
1456s		1503	1455	4.295	0.601	C-C-C ring vibration
1332vw	1329w	1383	1339	1.268	0.442	C-H in-plane bending vibration
1295vw		1348	1305	3.538	1.088	C-C-C ring vibration
1191w	1183w	1221	1181	0.961	3.096	C-N stretching; C-H stretching

1167m		1210	1171	8.782	17.123	C-N stretching
1123w		1187	1148	0.008	3.203	C-H out-plane bending
1110w		1136	1100	4.359	7.881	C-H, N-H, C-C stretching
1032vw	1027w	1085	1050	7.265	0.886	C-C-H in-plane bending
		1076	1041	7.491	3.202	NH_2 in-plane bending vibration
	1006s	1051	1017	2.668	13.382	C-C stretch + C-C-C ring vibration
994vw		1030	997	0.001	0.128	C-H out plane bending vibration
		1029	996	130.382	2.362	As-OH in plane bending
		1016	983	7.805	24.056	C-C-C in plane bending vibrtion
		996	964	0.105	0.019	C-H and N-H stretching
		968	937	73.294	1.864	OH stretching
		965	934	89.216	3.416	AsO_3 stretching
894vs	882vs	936	906	2.197	0.196	C-H out plane bending / C-C-O in plane bending vibration
863vs		885	856	38.518	30.376	AsO_3 stretching
	830m	858	831	0.831	0.693	C-H out plane bending
771vs		806	780	6.011	11.583	C-N stretching/C-C-C stretching
751vs	754vs	759	734	54.349	0.025	AsO_3 stretching
689s		711	688	20.272	0.782	C-C; C-H and N-H stretching
620vw	619vw	634	613	9.9215	6.716	C-C/C-H outplane bending
581w		562	544	79.911	6.701	NH_3 torsion/O-As-O deformation modes
531w	532vw	532	515	87.613	7.582	NH_3 torsion/O-As-O deformation modes
		522	505	55.253	2.556	H-N-H, H-O-H deformation
490m		519	502	64.592	2.029	H-N-H, H-O-H deformation
		488	473	51.410	0.184	H-N-H, H-O-H deformation
414s	407vw	428	414	48.302	0.504	O-As-O deformation; C-NH_3

						stretching
		419	406	0.051	0.086	C-C/C-H stretching
		382	370	74.944	4.669	O-H out-plane bending
		345	334	97.392	4.675	O-As-O deformation modes
		339	328	64.755	1.682	O-As-O deformation modes
		293	283	9.303	4.783	O-As-O deformation modes
	279w	288	279	73.059	0.351	O-As-O deformation modes
		270	261	0.060	2.029	O-As-O deformation modes/ring distortion
		261	253	0.141	1.364	O-As-O deformation modes/ring distortion
		223	216	30.502	0.243	O-As-O deformation modes/ring distortion
		172	167	22.826	0.835	L
		152	147	0.240	4.966	L
	84s	88	85	5.613	0.136	L
		68	66	1.116	0.560	L
		48	46	2.329	6.039	L
		41	40	0.241	1.004	L

Abbreviations: vs-very strong; s- strong, w-weak, v-very, sh-shoulder, b-broad, m-medium

Table 7. Second-order perturbation theory analysis of the Fock matrix in NBO basis calculated at B3LYP/6-311G(d.p) level.

Donor (i)	**Acceptor (j)**	**E$^{(2)}$ (Kj.mol^{-1})**	**E(j)-E(i) (a.u)**	**F(i.j) (a.u)**
Within unit 1				
σ(As1-O4)	σ*(As1-O7)	9.50	0.96	0.088
σ(As1-O7)	σ*(As1-O4)	9.30	0.96	0.087
LP*(1)As1	σ*(As1-O7)	11.91	0.27	0.084
LP*(1)As1	σ*(As1-O4)	9.98	0.27	0.077
LP(2)O4	LP*(1)As1	46.22	0.17	0.088
LP(3)O4	LP*(2)As1	60.34	0.18	0.104
LP(2)O7	LP*(1)As1	515.51	0.16	0.092
LP(3)O7	LP*(2)As1	65.99	0.18	0.108
From unit 1 to unit 2				
σ*(As1-O4)	σ*(O2-H3)	0.21	0.23	0.022
σ*(As1-O7)	σ*(O2-H3)	0.07	0.22	0.012
From unit 1 to unit 3				
σ*(As1-O4)	σ*(O5-H6)	0.32	1.18	0.017
LP*(1)As1	σ*(O5-H6)	0.94	0.50	0.036
σ*(As1-O4)	σ*(O5-H6)	0.21	0.23	0.022
σ*(As1-O7)	σ*(O5-H6)	0.07	0.22	0.012
From unit 1 to unit 4				
LP(2)O4	σ*(C21-H22)	4.58	0.71	0.053
σ*(As1-O4)	σ*(C21-H22)	0.43	0.27	0.032
From unit 2 to unit 1				
BD(1)O2-H3	LP*(2)As1	3.10	0.67	0.048
LP(1)O2	LP*(2)As1	12.69	0.43	0.077

LP(2)O2	LP*(1)As1	19.41	0.46	0.097
LP(3)O2	LP*(1)As1	119.09	0.42	0.212
LP(3)O2	LP*(2)As1	76.45	0.44	0.173
From unit 2 to unit 4				
LP(2)O2	σ*(N8-H10)	20.32	0.84	0.117
LP(1)O2	σ*(N8-H10)	3.07	0.79	0.044
From unit 3 to unit 1				
LP(1)O5	LP*(2)As1	12.69	0.43	0.077
LP(2)O5	LP*(1)As1	19.41	0.46	0.097
LP(3)O5	LP*(1)As1	119.09	0.42	0.212
LP(3)O5	LP*(2)As1	76.47	0.44	0.173
LP(3)O5	σ*(As1-O7)	9.01	0.69	0.074
From unit 3 to unit 4				
LP(2)O5	σ*(N8-H11)	20.31	0.84	0.117
LP(1)O5	σ*N8-H11)	3.07	0.79	0.044
Within unit 4				
π (C12-C13)	π *(C15-C17)	17.69	0.31	0.066
π(C15-C17)	π *(C12-C13)	22.09	0.27	0.069
π(C15-C17)	π *(C19-C21)	19.40	0.29	0.068
π(C12-C13)	π *(C19-C21)	18.73	031	0.069
π*(C12-C13)	π *(C15-C17)	175.32	0.02	0.083
π*(C12-C13)	π *(C19-C21)	122.28	0.02	0.083

Table 8. Electronic absorption spectrum obtained for ANILAS in different solvents and compared with the values calculated at B3LYP/6-311G(d,p) level of theory along with their excitation and assignments.

Solvents	**Excitation**	**Calc. Wavelength (nm)**	**Assignment**
Gas Phase	Homo → Lumo Homo → Lumo +1	242	LP(1) O15 - LP(2)O15
DMF	Homo → Lumo Homo → Lumo +1 Homo -1 → Lumo Homo -1 → Lumo +1	227	LP(1) O7 - LP(2) O7 LP(1) O7 - LP(3) O7 LP(3) O7 - LP(2) O7 LP(3) O7 - LP(3) O7
Water	Homo → Lumo Homo → Lumo +1 Homo -1 → Lumo Homo -1 → Lumo +1	227	LP(1) O7 - LP(2) O7 LP(1) O7 - LP(3) O7 LP(3) O7 - LP(2) O7 LP(3) O7 - LP(3) O7

Table 9. HOMO–LUMO energy value and related properties of ANILAS calculated at B3LYP /6-311G(d,p)method

E_{HOMO} (*eV*)	- 1.1486
E_{LUMO}(*eV*)	- 6.8390
Energy gap ΔE (*eV*)	5.6904
Ionization potential (A) *eV*	+1.1486
Electron affinity (I)	+6.8390
Global softness (S)	0.1757
Global hardness (**η**)	2.8452
Chemical potential (μ)	3.9938
Global electrophilicity (ω)	2.8030

Graphical Abstract